Rider Cooperative Control of Rear-Wheel-Swing Motorcycle based on Divergent Component of Motion

Tadashi Sumioka[1], Kazushi Akimoto[1], Takuya Tsujimura[1], Sho Takayanagi[1], Katsuhiko Fukushima[1], and Tsubasa Nose[2]

***Abstract*— We previously proposed a motorcycle with a balance assist function that can generate a self-balancing moment by changing the front wheel fork slant angle. Although this method reduces the risk of falling over, it makes it difficult for the rider to go in the desired direction due to interference by the front wheel assist. In order to solve this problem, this paper proposes a rear-wheel-swing assist mechanism that minimizes the influence on the front wheel steering operation. A method for realizing cooperative control with the rider using the divergent component of motion is also proposed. The results of an extremely low-speed U-turn test are used to show that the proposed methods provide stability while maintaining drivability.**

I. Introduction

Motorcycles are attractive vehicles because they are small and highly maneuverable. However, they are unstable when stopped or moving at extremely low speeds, so riders have to maintain roll balance, which is difficult for beginners, people with small physiques, and elderly riders. Many studies have been conducted on the stability of motorcycles (e.g., [1], [2], [3]); however, few studies have considered the extremely low-speed range. Research on the stability of motorcycles in the extremely low-speed range (e.g., [4], [5]) has mainly focused on analysis and simulation, with few examples of the implementation of stabilization in actual motorcycles. We previously proposed a motorcycle with a balance assist function that is effective in the extremely low-speed range [6]. This motorcycle, based on an equivalent two-point mass decomposition (E2PMD) model, adjusts the trail length by changing the front wheel fork slant angle to generate a self-balancing moment without the large flywheel or balancer used in conventional motorcycle robots (e.g., [7], [8]). Although this method reduces the risk of falling over, it makes it difficult for the rider to go in the desired direction due to interference by the front wheel assist. In order to overcome this problem, this paper proposes a rear-wheel-swing assist mechanism, shown in Fig. 1, that minimizes the influence on the rider's steering operation. The balance assist control of the motorcycle must match the rider's intentions. Specifically, when the rider leans into a turn, the balance assist control should not resist the rider, and when the rider tries to maintain roll balance by steering, accelerating, decelerating, or shifting weight etc., it should not provide excessive support, which would degrade drivability. However, little research has been done on the coordination between the balance assist control and the rider. Tsujii et al. have proposed a mechanism to stabilize the motorcycle by adding a rotation axis to the rear wheel to control the position of the center of gravity, but there is no mention of how to cooperate with the rider [9]. To investigate the human sense of balance, Zhang, Wang, Yi, and Chen et al. installed a gyroscope balancer on a bikebot and controlled and analyzed the roll stability of the system (rider and bikebot) as a whole [10]- [12]. However, their studies did not consider drivability and cooperation with the rider. Since motorcycle riding techniques can vary due to several factors (e.g., the rider ' s skill and physique), creating a model for riders and accurately estimating their state is considered challenging. Therefore, when trying to obtain the rider's state for rider cooperative control, it is necessary to add a new measuring instrument as in previous research [10]. However, it is not desirable from a cost perspective. Based on the above, in order to achieve cooperative control between a rider and a motorcycle, we considered it to be reasonable to use roll balance assist control when it is truly necessary, for instance, there is a high risk of falling.

Fig. 1. Motorcycle with rear-wheel-swing assist mechanism. This experimental vehicle was developed based on a mass-produced motorcycle

Various stabilization control methods and analysis methods have been proposed for biped robots that stabilize unstable objects such as motorcycles . Among them, we have focused on the divergent component of motion (DCM) [13] as a method to analytically calculate the risk of falling. DCM, proposed by Takenaka et al. [13]- [16], guarantees the continuity of the gait of a biped robot and theoretically relaxes the boundary value problem. It has been used in many biped robots (e.g., [17]- [21]). Moreover, the extrapolated center of mass position (XcoM) [22], which is a concept equivalent to DCM, has been proposed as an indicator of the

This paper was recommended for publication by Editor Angelika Peer upon evaluation of the Associate Editor and Reviewers ' comments.

[1]Tadashi Sumioka, Kazushi Akimoto, Takuya Tsujimura, Sho takayanagi and Katsuhiko Fukushima are with Honda R&D Co., Ltd., Innovative Research Excellence, Frontier Robotics, Saitama 3510193, Japan tadashi_sumioka@jp.honda

[2] Tsubasa Nose is with Honda R&D Co.,Ltd. Strategy Department, Planning Division, Corporate Development Center ., Tokyo 1510051, Japan

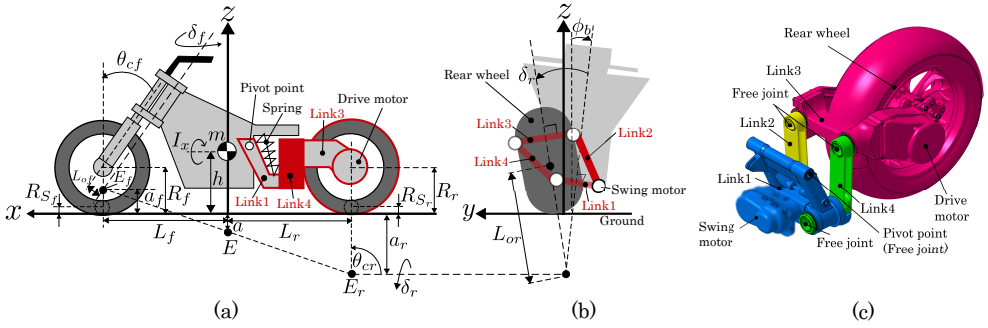

Fig. 2. Hardware configuration of motorcycle with proposed rear-wheel-swing assist mechanism. (a) Left-side view. (b) Rear view. (c) Details of the four-bar-linkage mechanism. The rear wheel is swung using a four-bar linkage mechanism, where the length of the link3 is longer than that of the link1, and link2 and link4 are the same length. The vehicle body is fixed to the link1 and the rear wheel is fixed to the link3. The link1 is connected to the vehicle body at the pivot point. δ_r is the rear-wheel-swing angle, which is the same as the rear wheel roll angle with respect to the vehicle body. Although θ_{cr} and L_{or} are extremely large, δ_r can also be considered the steering angle of the rear wheel in a broad sense based on the same definition as the front wheel.

balance control of the human body. Sugihara showed that it is possible to analytically obtain the state quantity range in which a biped robot can be stabilized using the best center of mass/zero-moment point regulator that is equivalent to DCM feedback control [23]. A rider can control a motorcycle within a certain state range, so it is useful to obtain such a stabilizable range. For biped robot control, an object can be approximated as a linear inverted pendulum (LIP) model. An LIP model can also be derived for motorcycle control. However, there is no LIP model for which large front and rear wheel steering angles are assumed when a motorcycle is stopped or moving at extremely low speeds.

Therefore, we define an E2PMD model that can be applied to a motorcycle that has the front and rear wheel steering shown in Fig. 1. We then derive an E2PMD-LIP model similar to the model used for biped robots. The LIP model of a biped robot has the following input constraint: the zero-moment point can only exist in the foot support polygon. An E2PMD-LIP model can be modeled as an LIP model with input constraints, considering that the steering angles of the front and rear wheels have a fixed range.

We propose a method that achieves both roll stability and drivability by evaluating the margin of the current state quantity from the limit state quantity that can be stabilized and adjusts the assist effect according to the margin size. As a representative example of the benefits of the proposed balance assist, we show the results of an extremely low-speed U-turn test.

II. Experimental Hardware and Overall Control Scheme

The hardware configuration of the motorcycle used in this paper is shown in Fig. 2. The variables used in this paper are defined in Table I. As shown in Fig. 2, the rear wheel is swung using a four-bar linkage. That is, the rear wheel can be swung by fixing the vehicle body to the link1 and fixing the rear wheel to the link3. θ_{cr} is set to be slightly smaller than $\pi/2$ rad. The rear-wheel-swing motor has a configuration that can control the motor angular velocity. The rear wheel is driven by a motor. The following values are measured using sensors for control:

- Front wheel speed.
- Front steering angle.
- Rear-wheel-swing motor angle.
- Three-axis acceleration and three-axis angular velocity of vehicle body (six-axis inertial measurement unit).

If the specifications of the base vehicle deviates significantly from the required standards, it may become difficult to drive and evaluate the proposed method. Therefore, we designed the test vehicle to ensure that m, L_r, h, I_x, etc. do not deviate from the values of mass-produced motorcycle [1]. The sampling period is 0.001 s.

Fig. 3 shows the overall diagram of the control scheme proposed in this paper. Each block in Fig. 3 is described in detail in the following sections.

TABLE I
Definition of Variables

Symbol	Unit	Description
m	kg	Total mass
h	m	Height of center of gravity
I_x	kgm^2	Total roll inertia about center of gravity
g	m/s^2	Gravitational acceleration
δ_i	rad	Steering angle
R_i	m	Wheel radius
R_{S_i}	m	Wheel sectional radius
θ_{ci}	rad	Caster angle
L	m	Wheel base
L_i	m	Length from wheel axle to center of gravity
L_{oi}	m	Fork offset
a_i	m	Displacements of E_i in z-axis direction
ϕ_b	rad	Roll angle of vehicle body (lean angle)
ϕ_i	rad	Roll angle of wheel

$i \in \{f, r\}$, f denotes the front wheel and r denotes the rear wheel

[1]The base motorcycle is a Honda NM4, which is no longer in production.

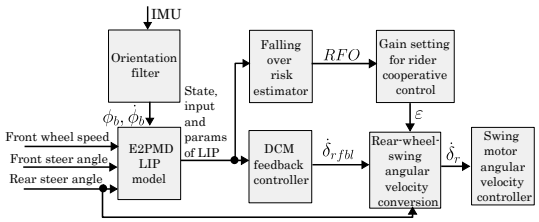

Fig. 3. The overall diagram of the control scheme

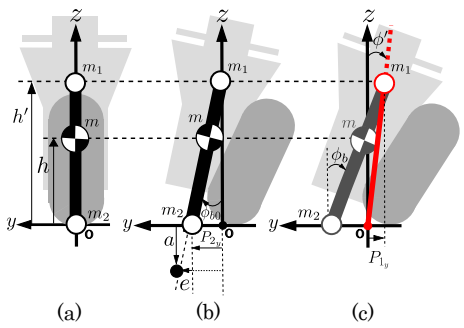

Fig. 4. Approximate dynamics model of equivalent two-point mass system. (a) Reference attitude. (b) Approximate dynamics model that ignores change in angular momentum due to gravity term. The second point mass moves and the roll angle changes as a result of the steering operation. (c) Roll angle of first point mass in model that considers gravitational term, inertial force term, and vehicle body roll angle.

III. Two-point mass decomposition/linear inverted pendulum model for vehicle with front and rear wheel steering

This section shows that E2PMD [6] can be used to model the roll dynamics of a vehicle with front and rear wheel steering as a simple LIP. Here, the state in which the vehicle stands upright at the straight-ahead attitude is referred to as the "reference attitude". The coordinates are set as follows:

- The front and rear wheel steering angles and the roll angle are set to zero when the vehicle is in the reference attitude.
- The origin of the coordinate system is placed at the projected point on the ground of the center of gravity of the vehicle in the reference attitude. The resulting Cartesian coordinate system has x, y, and z axes in a right-handed system.
- In the reference attitude, E_i is the point of intersection between the line that connects the center of the wheel and the grounding point of the wheel and the line of the steering axis.
- Let E be the intersection of the straight line through E_f and E_r and the z axis.

In the reference attitude, when the whole vehicle is represented by a rigid point mass, the resulting system can be converted to the equivalent system shown in Fig. 4(a), which consists of a point mass at a height above the center of gravity height h (mass m_1 at height h') and a second point mass on the ground (mass m_2 at height 0). P_{1_y} is the lateral displacement of the first mass point, which is the state variable of the E2PMD-LIP model. For this system, the following relational expressions are valid:

$$m = m_1 + m_2, \tag{1}$$
$$m_1 (h' - h) = m_2 h, \tag{2}$$
$$m_1 (h' - h)^2 + m_2 h^2 = I_x. \tag{3}$$

From (1) through (3), m_1, m_2, and h' can be obtained. It is assumed that the initial roll angular velocity is set to zero, the change in angular velocity due to gravitational acceleration is negligible, and the mass points are constrained to move horizontally. The position of the second mass point is thus uniquely determined by the steering angles of the front and rear wheels. Moreover, since the height of the second mass point is 0, no angular momentum is generated even if the second mass point moves. According to the law of conservation of angular momentum, the first mass point does not move. That is, the first point mass can be regarded as a fixed point for steering when the gravity term is ignored. As a result, the vehicle body rotates in the roll direction around the first mass point. The roll angle generated around the first mass point by steering is ϕ_{b0} and the displacement of the second mass point in the y-axis direction is P_{2_y}. ϕ_{b0} and P_{2_y} are important in deriving the input term of E2PMD-LIP model. Under the assumption that ϕ_{b0} is sufficiently small, P_{2_y} can be expressed as

$$P_{2_y} = h' \phi_{b0}. \tag{4}$$

The roll angles of the front and rear wheels can be approximated as

$$\phi_i \simeq \phi_{b0} - \delta_i \sin\theta_{ci}. \tag{5}$$

The displacements of E_f and E_r in the y-axis direction, e_f and e_r, respectively, are

$$e_i = -a_i \phi_i, \tag{6}$$

where a_f and a_r are geometrically obtained as

$$a_f = R_f - \frac{L_{of}}{\sin\theta_{cf}}, \tag{7}$$
$$a_r = R_r - \frac{L_{or}\cos\delta_r}{\sin\theta_{cr}} \simeq R_r - \frac{L_{or}}{\sin\theta_{cr}}. \tag{8}$$

In addition, the displacement of E in the z-axis direction, a, is

$$a = \frac{L_r}{L} a_f + \frac{L_f}{L} a_r. \tag{9}$$

Similarly, the displacement of E in the y-axis direction, e, is

$$e = \frac{L_r}{L} e_f + \frac{L_f}{L} e_r. \tag{10}$$

From the geometric relationship shown in Fig. 4(b), P_{2_y} can be expressed as

$$P_{2_y} = e + a\phi_{b0}. \tag{11}$$

From (4) to (11), ϕ_{b0} and P_{2_y} can be respectively obtained as

$$\phi_{b0} = \frac{L_r a_f \sin\theta_{cf}}{Lh'}\delta_f + \frac{L_f a_r \sin\theta_{cr}}{Lh'}\delta_r, \quad (12)$$

$$P_{2_y} = \frac{L_r a_f \sin\theta_{cf}}{L}\delta_f + \frac{L_f a_r \sin\theta_{cr}}{L}\delta_r. \quad (13)$$

Fig. 4(c) shows a model that considers the effects of the gravity term and the inertial force. The angular momentum of the equivalent two-point mass system changes due to gravity acting on the first and second point masses and the floor reaction force acting on the contact points on the ground. Since the position of the second point mass is uniquely determined by the front and rear wheel steering angles, the angular momentum of the first point mass coincides with the angular momentum of the equivalent two-point mass system. In this system, the first-point-mass roll angle is defined as ϕ'. The following relationship exists among ϕ', ϕ_b, and ϕ_{b0}:

$$\phi' = \phi_b - \phi_{b0}. \quad (14)$$

The elements of the roll moment generated in the system shown in Fig. 4(c) are as follows:

- Moment of inertia acting on m_1: $m_1 h'^2 \ddot{\phi}'$
- Gravity moment acting on m_1: $m_1 g h' \phi'$
- Gravity moment acting on m_2: $-m_2 g P_{2_y}$
- Ground reaction moment generated by vehicle body roll: $-mgR_{S_{eq}}\phi'$
- Ground reaction moment due to front and rear wheel steering: $mgP_{rpt_{oy}}$
- Inertial force moment of m_1 due to coordinate origin acceleration: $m_1 h' \left(\dot{V}_{oy} + V_{ox}\omega_z\right)$

where $R_{S_{eq}}$ is defined as the following equivalent sectional radius of a wheel:

$$R_{S_{eq}} = \frac{L_r}{L}R_{S_f} + \frac{L_f}{L}R_{S_r}. \quad (15)$$

In addition, $P_{rpt_{oy}}$, which is the amount of movement of the grounding point generated by steering, can be calculated as

$$P_{rpt_{oy}} = \frac{L_r R_{S_f} \sin\theta_{cf}}{L}\delta_f + \frac{L_f R_{S_r} \sin\theta_{cr}}{L}\delta_r - R_{S_{eq}}\phi_{b0}. \quad (16)$$

V_{ox}, V_{oy}, and ω_z denote the longitudinal velocity, lateral velocity, and yaw rate at the center of gravity of the vehicle, respectively. Under the assumption that the effect of the side slip angle is negligible at low speeds, V_{oy} and ω_z are respectively expressed as

$$V_{oy} = \frac{L_r V_{ox}\cos\theta_{cf}}{L}\delta_f + \frac{L_f V_{ox}\cos\theta_{cr}}{L}\delta_r, \quad (17)$$

$$\omega_z = \frac{V_{ox}\cos\theta_{cf}}{L}\delta_f - \frac{V_{ox}\cos\theta_{cr}}{L}\delta_r. \quad (18)$$

Under the assumption that ϕ' is sufficiently small, P_{1_y} is defined as

$$P_{1_y} = -h'\phi'. \quad (19)$$

From (12) to (19), the dynamics of the E2PMD-LIP model are represented by the following state equation:

$$\frac{d}{dt}\begin{bmatrix} P_{1_y} \\ \dot{P}_{1_y} \end{bmatrix} = \begin{bmatrix} 0 & 1 \\ \omega^2 & 0 \end{bmatrix}\begin{bmatrix} P_{1_y} \\ \dot{P}_{1_y} \end{bmatrix} + \begin{bmatrix} 0 \\ -1 \end{bmatrix} u, \quad (20)$$

where

$$\omega^2 = \left(1 - \frac{m}{m_1 h'}R_{S_{eq}}\right)\frac{g}{h'}, \quad (21)$$

$$u = \dot{V}_{oy} + V_{ox}\omega_z - \frac{g}{h'}\frac{m_2}{m_1}P_{2_y} + \frac{g}{h'}\frac{m}{m_1}P_{rpt_{oy}}. \quad (22)$$

From the above, u is a function with variables $\dot{V}_{ox}$, V_{ox}, $\dot{\delta}_f$, δ_f, $\dot{\delta}_r$, and δ_r. Since L_{or} is a nonlinear function of δ_r, u is also a nonlinear function of δ_r. From (12), (13), (14) and (22), it can be seen that as a_r, which affects the rear-wheel swing radius, increases, both the lateral movement amount of the LIP and the generated restoring force also increase.

IV. Rider-machine cooperative control

The rear wheel is swung such that the control input u satisfies the following:

$$u = K_P\left(P_{1_y} - P_{1_{y_d}}\right) + K_V\left(\dot{P}_{1_y} - \dot{P}_{1_{y_d}}\right), \quad (23)$$

where $P_{1_{y_d}}$ is the desired value of P_{1_y} and the equilibrium of the E2PMD-LIP model when $\delta_r = 0$. $\dot{P}_{1_{y_d}}$ is the desired value of $\dot{P}_{1_y}$ and is obtained via the pseudo-differentiation of $P_{1_{y_d}}$.

A. Divergent component of motion feedback control

To determine the control gains K_P and K_V in (23), we apply the concept of DCM feedback control. The content of this section does not lose its generality even if $P_{1_{y_d}} = \dot{P}_{1_{y_d}} = 0$ because the coordinate transformation should be performed such that the origin becomes the desired state. Therefore, in the remaining parts, unless otherwise specified, $P_{1_{y_d}} = \dot{P}_{1_{y_d}} = 0$ for simplicity.

1) Divergent component of motion: We now review the characteristics of the DCM described in [13], [17] and [23]. The new input p of the E2PMD-LIP model is defined as

$$p = \frac{u}{\omega^2}. \quad (24)$$

By substituting (24) into (20), the equation of state can be rewritten as

$$\frac{d}{dt}\begin{bmatrix} P_{1_y} \\ \dot{P}_{1_y} \end{bmatrix} = \begin{bmatrix} 0 & 1 \\ \omega^2 & 0 \end{bmatrix}\begin{bmatrix} P_{1_y} \\ \dot{P}_{1_y} \end{bmatrix} + \begin{bmatrix} 0 \\ -\omega^2 \end{bmatrix} p. \quad (25)$$

Equation (25) is equivalent to the LIP model used for a biped robot [13] by defining p as the zero-moment point and P_{1_y} as the center of gravity. For a biped robot, the natural frequency is $\sqrt{g/h}$. An E2PMD-LIP model has a coefficient, such as $1 - (m/m_1 h')R_{S_{eq}}$. The system matrix of (25) has eigenvalues $\pm\omega$ and its eigenvectors are, for example, $\boldsymbol{v}_n = [0.5, -0.5\omega]^T$ and $\boldsymbol{v}_p = [0.5, 0.5\omega]^T$. A linear state transformation is obtained as follows:

$$\begin{bmatrix} \eta \\ \xi \end{bmatrix} = [\boldsymbol{v}_n, \boldsymbol{v}_p]^{-1}\begin{bmatrix} P_{1_y} \\ \dot{P}_{1_y} \end{bmatrix}. \quad (26)$$

By substituting the derivative of the (26) into (25), the dynamics can be diagonalized as

$$\frac{d}{dt}\begin{bmatrix}\eta\\ \xi\end{bmatrix} = \begin{bmatrix}-\omega & 0\\ 0 & \omega\end{bmatrix}\begin{bmatrix}\eta\\ \xi\end{bmatrix}. \tag{27}$$

(27) shows that η will converge and ξ will diverge by time evolution. Therefore, η is called the convergence component of motion (CCM) and ξ is called DCM. From (26), ξ is as follows:

$$\xi = P_{1_y} + \frac{\dot{P}_{1_y}}{\omega}. \tag{28}$$

2) Gain setting for divergent component of motion feedback control: In order to suppress excessive control intervention and realize natural control, we use only DCM for feedback control and ignore the CCM that naturally converges. Using (28), DCM feedback control is

$$u = K_\xi \xi = K_\xi P_{1_y} + \frac{K_\xi}{\omega}\dot{P}_{1_y}. \tag{29}$$

If $K_P = K_\xi$ and $K_V = K_P/\omega$, the above equation is in the form of (23). In other words, DCM feedback control is equivalent to setting K_P and K_V to satisfy $K_P/K_V = \omega$. Substituting $u = K_P P_{1_y} + (K_P/\omega)\dot{P}_{1_y}$ into (20) yields the following poles of the system:

$$p_1 = -\omega, \tag{30}$$

$$p_2 = -\frac{K_P - \omega^2}{\omega}. \tag{31}$$

In other words, DCM feedback control is equivalent to setting one of the poles to $-\omega$.

3) Falling over risk under divergent component of motion feedback control: Roll stability analysis during DCM feedback control is performed using the concept of the best center of mass/zero-moment point regulator proposed by Sugihara [23]. For a biped robot, the zero-moment point input p in (25) is saturated at a certain value because of the supporting region constraint of the foot. When calculating the control input for stabilization using the right-hand side of (23) for a motorcycle, the control input follows the right-hand side of (22). However, this value saturates at a certain value because the front and rear wheel steering angles have a fixed range. Hence, the actual u is

$$u = \begin{cases} u_{min} & (u < u_{min}) \\ K_P P_{1_y} + \frac{K_P}{\omega}\dot{P}_{1_y} & (u_{min} \le u \le u_{max}) \\ u_{max} & (u > u_{max}) \end{cases}. \tag{32}$$

Here u_{min} and u_{max} denote the lower and upper limits of u, respectively. Under the assumption that $\dot{V}_{ox} = 0$, $\dot{\delta}_f = 0$, and $\dot{\delta}_r = 0$, u_{min} is obtained by setting $\delta_f = \delta_{f_{min}}$ and $\delta_r = \delta_{r_{min}}$ when calculating the right-hand side of (22). Similarly, u_{max} is obtained by setting $\delta_f = \delta_{f_{max}}$ and $\delta_r = \delta_{r_{max}}$ when calculating the right-hand side of (22). Since u depends on V_{ox}, u_{min} and u_{max} also depend on V_{ox}. Here, from(24), when $u = u_{min}$, $p = p_{min} = u_{min}/\omega^2$. Similary, when $u = u_{max}$, $p = p_{max} = u_{max}/\omega^2$. Fig. 5 shows the phase portrait using (32). Fig. 5(a) and 5(b) show the phase portrait for a vehicle speed of 0 and 0.694 m/s, respectively. As the vehicle speed increases, the input limit values $|u_{min}|$ and $|u_{max}|$ increase and the area that can be stabilized increases. It can also be seen that setting the gain ratio to $K_P/K_V = \omega$ is equivalent to making the state feedback controllable area parallel to the CCM separatrix. Making the state feedback control region parallel to the CCM separatrix maximizes the margin from the state feedback controllable area to the DCM separatrix and stabilizes all states starting from within the state feedback controllable area. Even if the state quantity outside the state feedback control region, it can be stabilized by entering the state feedback region if it is within the CCM separatrix. Therefore, DCM feedback control can stabilize the vehicle if the state quantity is within the CCM separatrix. Note that DCM is p_{max} when the state quantity is on the CCM separatrix through p_{max}. Similarly, DCM is p_{min} when the state quantity is on the CCM separatrix through p_{min}. Here, Risk of Falling Over (RFO) is defined as the normalized value of how much the current DCM has a margin compared to the DCM on the CCM separatrix.

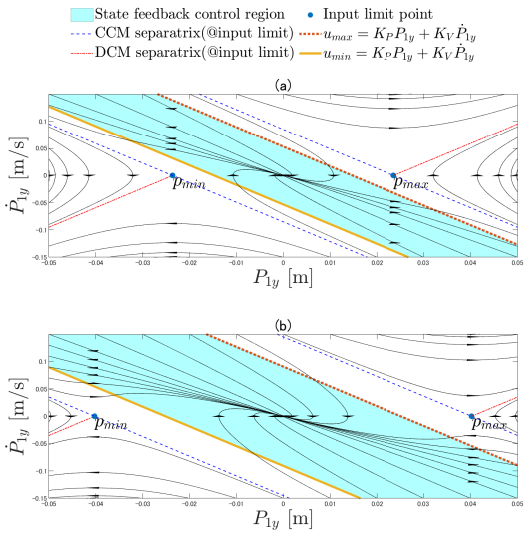

Fig. 5. Phase portrait of model with DCM feedback control. Here, $\omega^2 = 13$, $K_P = 20.8$, and $K_V = K_P/\omega$. (a) $V_{ox} = 0$ m/s, $u_{min} = -0.3072, u_{max} = 0.3072$. (b) $V_{ox} = 0.694$ m/s, $u_{min} = -0.5233, u_{max} = 0.5233$. Note that as V_{ox} increases, $|p_{min}|$ and $|p_{max}|$ also increase, and the area that can be stabilized increases.

$$RFO = \frac{|\xi(t)|}{|\xi_{lim}|}, \tag{33}$$

where $\xi(t)$ and ξ_{lim} represent the DCM at the current time and that at p_{min} or p_{max}, respectively. Under the assumption that the allowed steering angles on the left and right are equal, $|\xi_{lim}| = |p_{max}| = |p_{min}|$. If RFO is greater than 1, the vehicle can become unstable. Therefore, if RFO is small to some extent, decrease the control gain shown in the next section for the maneuverability as perceived by the rider, and if RFO is close to 1, increase the control gain to help with falling over avoidance. As described above, RFO is used as an index for realizing cooperative control with the rider.

From Fig. 5(a) and 5(b), when the state quantity is the same value, the RFO in Fig. 5(b), which has a higher vehicle speed, is smaller. Therefore, the control gain is lower for a higher vehicle speed, giving priority to maneuverability.

B. Rear-wheel-swing angular velocity for feedback linearization

The rear-wheel-swing angular velocity was calculated such that the right-hand side of (22) and the right-hand side of (23) are equal. The following is obtained by a first-order approximation of (22) by Taylor expansion around the point one sampling period before:

$$\begin{aligned} u &\simeq u_p + \frac{\partial u}{\partial \delta_r}\left(\delta_r - \delta_{r_p}\right), \\ &= u_p + \frac{\partial u}{\partial \delta_r}\Delta t \dot{\delta}_r, \end{aligned} \tag{34}$$

where u_p and δ_{r_p} are u and δ_r in the previous sampling period, respectively, and Δt is the sampling period. From (23) and (34), the rear wheel steering angular velocity input $\dot{\delta}_{r_{fbl}}$ that realizes the feedback linearization is

$$\dot{\delta}_{r_{fbl}} = \frac{K_P P_{1_y} + \frac{K_P}{\omega}\dot{P}_{1_y} - u_p}{\frac{\partial u}{\partial \delta_r}\Delta t}. \tag{35}$$

Here, u_p is used as the control input in the previous sampling period. It was confirmed that there is no practical problem if the sampling period is short. The rear-wheel-swing motor angular velocity is calculated from the rear-wheel steering angular velocity in consideration of the four-bar linkage mechanism and reduction ratio.

C. Rear-wheel-swing angular velocity command value considering rider operation

Using (35), the system can be approximated by

$$\frac{d}{dt}\begin{bmatrix} P_{1_y} \\ \dot{P}_{1_y} \end{bmatrix} = \begin{bmatrix} 0 & 1 \\ \omega^2 - K_P & -\frac{K_P}{\omega} \end{bmatrix}\begin{bmatrix} P_{1_y} \\ \dot{P}_{1_y} \end{bmatrix}. \tag{36}$$

In the above system, all rider inputs are canceled and stabilized so the control may interfere with the rider's intention, making the rider feel a loss of control. Therefore, we consider using the following rear-wheel-swing angular velocity to maintain the rider's control:

$$\dot{\delta}_r = \varepsilon \dot{\delta}_{r_{fbl}} + (1-\varepsilon) K_{r0}\delta_r, \tag{37}$$

where K_{r0} is a negative constant and $\varepsilon \in [0, 1]$. When $\varepsilon = 1$, $\dot{\delta}_r = \dot{\delta}_{r_{fbl}}$ and it can be stabilized by feedback linearization. When $\varepsilon = 0$, $\dot{\delta}_r = K_{r0}\delta_r$ and the rear-wheel swing angle can be asymptotically zero. As shown in Fig. 6, ε takes a value near 0 to give priority to maneuvering when RFO is low, and takes a value near 1 to prioritize stability when RFO is high. Substituting (34), (35), and (37) into (20) yields

$$\begin{aligned} \frac{d}{dt}\begin{bmatrix} P_{1_y} \\ \dot{P}_{1_y} \end{bmatrix} &= \begin{bmatrix} 0 & 1 \\ \omega^2 - \varepsilon K_P & -\frac{\varepsilon K_P}{\omega} \end{bmatrix}\begin{bmatrix} P_{1_y} \\ \dot{P}_{1_y} \end{bmatrix} \\ &+ \begin{bmatrix} 0 \\ -1 \end{bmatrix} u', \end{aligned} \tag{38}$$

$$u' = (1-\varepsilon)\left(u_p + \frac{\partial u}{\partial \delta_r}\Delta t K_{r0}\delta_r\right). \tag{39}$$

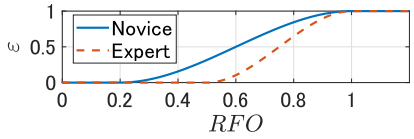

Fig. 6. ε-RFO setting example. For novice riders, it is advisable to use rear-wheel assist even if RFO is somewhat low. In the case of an experienced riders, it is better to have the assist intervene after RFO reaches a certain level to maintain drivability.

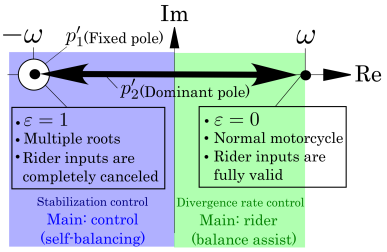

Fig. 7. Interpretation of proposed method for pole placement (for case with $K_P = 2\omega^2$).

The eigenvalues of the system matrix in (38) are

$$p_1' = -\omega, \tag{40}$$

$$p_2' = -\frac{\varepsilon K_P - \omega^2}{\omega}. \tag{41}$$

From (40) and (41), one can fix the pole p_1' at $-\omega$ and move the pole p_2' on the real axis by varying the value of ε between 0 and 1. When $\varepsilon < 1$, it can be seen from (39) that the rider's input term becomes dominant. From (41), if ε is set to a small value, $\varepsilon K_P < \omega^2$ and the pole exists in the right half of the complex plane. That is, p_2' becomes an unstable pole. Even if p_2' is in the right half-plane, but less than ω, the vehicle is assisted to tilt at a slower rate than the normal vehicle tilt speed. In addition, since the rider's input term also makes a contribution, the rider can easily stabilize the vehicle. The above discussion is summarized in Fig. 7. When the pole is in the right half-plane, the phase portrait is not that in Fig. 5, so the risk of falling over cannot be strictly calculated. However, Fig. 5 can be regarded as the phase portrait when the best operation is performed in terms of roll balance stabilization, so we consider RFO as an index of the risk of falling over even when the pole is in the right half-plane.

V. Experiment

Since making a U-turn at extremely low speed can lead to a fall, five authors conducted a U-turn test with a target vehicle speed of 3 km/h ($\simeq$ 0.8333 m/s). The U-turn course consisted of a 5 m straight line, a left semicircular turn with a 4.5 m radius, and another 5 m straight line. The range of δ_r was set to ± 1 deg ($\simeq$ 0.0175 rad). We conducted the test using a normal electric motorcycle without balance assist and a motorcycle with the proposed balance assist,

Fig. 8. Experiment scene. The target trajectory is marked with tape.

repeating it three times, and compared the results. [2] Fig. 8 shows photograph during the experiment.

A. Results

The comparative driving results of one rider are shown in Fig. 9. Here, $\delta_{r_{min}} = \delta_{r_{max}} = 0$ for calculating RFO for the normal electric motorcycle. The results for the proposed method at various distance intervals are summarized below.

Between 0 and 2 m
: RFO is high because the motorcycle speed is very low; the rear-wheel swing assist is active.

Between 2 m and 5 m
: RFO is low because the motorcycle is moving in a straight line; the rear-wheel swing assist is inactive.

Between 5 m and 19 m
: RFO is high because the motorcycle is turning; the rear-wheel swing assist is active.

Over 19 m
: Since deceleration starts when the front wheel is steered to a certain degree, RFO is high even when the motorcycle is moving in a straight line; the rear-wheel-swing assist is active.

The results of other riders showed a similar trend. In addition, as shown in Fig. 9(c), for the normal electric motorcycle, the steering is frequently corrected to maintain balance. The proposed method removes the need for these frequent corrections, reducing the rider's operation load for balancing. As shown in Fig. 10, the high-frequency component of δ_f is considered to be the corrected steering amount [24]. Therefore, considering $\delta_f(t)$ over a time interval $[t_e, t_s]$, we use the following Front Steering Correction(FSC) index as

$$FSC = \frac{1}{t_e - t_s} \int_{t_s}^{t_e} |HPF(\delta_f(t))| dt. \tag{42}$$

Here, HPF is a high-pass filter. Fig. 11 summarizes the average RFO value and FSC of all riders. The results show that by using the proposed method, RFO and FSC can be reduced for all riders. Averaging all trials for all riders, RFO can be reduced from 0.68 to 0.34(50% reduction), and FSC can be reduced from 0.13 rad to 0.09 rad(33% reduction) by using the proposed method. Table. II shows the results of analysis of variance(ANOVA) performed on

[2]We also attempted a comparison with a controller that does not consider the rider cooperative controller, that is, with ε fixed at 1. However, since it was difficult to lean the vehicle body when turning, most riders ended up going far off the course.

TABLE II

p-VALUES OF TWO-WAY ANOVA

	Rider's effect	Assist effect	Interaction
RFO	0.0000	0.0000	0.0007
FSC	0.0000	0.0000	0.4138

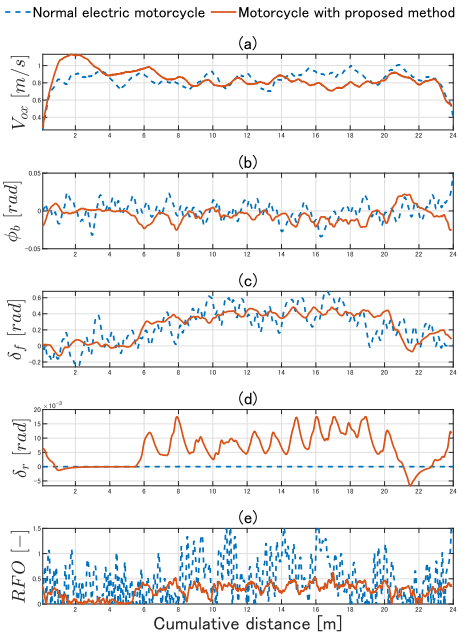

Fig. 9. Results of U-turn test. (a) Velocity. (b) Vehicle body roll angle. (c) Front steering angle. (d) Rear steering angle. (e) Risk of falling over. These data are unfiltered. The distance from 0 m to 5 m is a straight line, from 5 m to 19 m forms a leftward circle with a radius of 4.5 m, and from 19 m to 24 m is a straight line.

the experimental results. Table. II indicates that rider and assist affect the FSC and RFO, and regarding RFO, there is evidence of an interaction effect of the two. In particular, it is confirmed that the assist effect tends to be large for novice riders.

B. Discussions

Since the method proposed in this paper sets the caster angle of the rear wheel to slightly less than $\pi/2$ rad, even $\delta_r \neq 0$, the kinematic steering angle($\simeq \delta_i \cos\theta_{ci}$) of the rear wheel is small and has the same phase as the actual steering angle of the front wheel. Therefore, it is easy to control stability and minimize the influence on the rider's steering operation during driving. In the method proposed by Tsujii et al. [9], the added rotation axis corresponds to setting a rear wheel caster angle of 3/4π to 2π rad. As a result, the actual kinematic steering angles of the front and rear wheels are in opposite phase during roll stabilization assist, and the vehicle body roll moment generated by the front and rear wheel steering cancels out, making it difficult to stabilize the vehicle during turning.

Although the assist effects were confirmed, we did not explicitly consider the roll moment generated in the vehicle

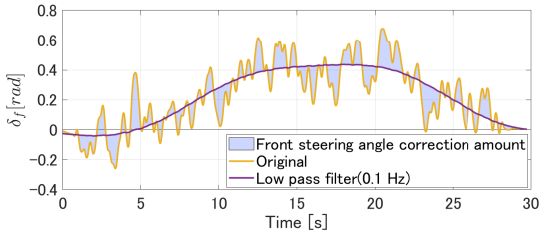

Fig. 10. Evaluation of front steering correction amount. This is the result when the rider operates the normal electric motorcycle without balance assist. It can be seen that in this driving mode, high-frequency corrective steering can be evaluated by setting the cutoff frequency to 0.1 Hz.

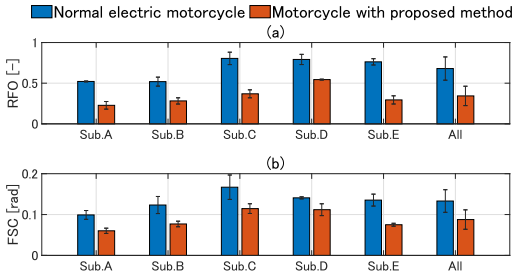

Fig. 11. Comparison results of quantitative evaluation indicators. (a) Mean and standard deviation of RFO. (b) Mean and standard deviation of FSC.

body due to the rider's handlebar operation and weight shift. Therefore, we did not verify stability considering the rider's roll moments when the pole is set on the right half of the complex plane. Furthermore, since the motorcycle riding technique varies depending on several factors (e.g., the rider's skill and physique), the effectiveness of the proposed method should be studied further by increasing the number of subjects and test patterns. In addition, in order to confirm the effectiveness of the proposed method, a method for quantitatively evaluating the assist effect and drivability should be developed.

VI. Conclusion

In this paper, we proposed a motorcycle with rear-wheel-swing balance assist that minimizes the influence on the front wheel steering operation. In addition, we applied DCM feedback control, which was proposed for biped robot control, to a motorcycle and proposed a control method that considers the risk of falling over. The main contribution of this paper is to propose a motorcycle assist method that uses these methods to reduce the risk of falling over while reducing the rider's operational load.

References

[1] R. S. Sharp, The stability and control of motorcycles, J. Mech. Eng. Sci, vol. 13, no. 5, pp. 316-329, May 1971.
[2] V. Cossalter, Motorcycle dynamics, 2nd ed. Morrisville, NC: Lulu Press, 2006.
[3] M. Tanell, M. Corno, and S. M. Savaresi, Modelling, simulation and control of two-wheeled vehicles. WILEY, 2014.
[4] S. Singhania, I. Kageyama, and V. M. Karanam, Study on low-speed stability of a motorcycle, MDPI, Advances in Mechanical Systems Dynamics, vol. 9, no. 11, pp. 78-92, 2019.
[5] V. D. Rosso, A. Andreucci, S. Boria, M. L. Corradini, R. Giambo, and A. Ranalli, Self-balancing electric motorcycle modelling at low speed: preliminary results, presented at 6th European Conference on Computational Mechanics, UK: Glasgow , June 2018.
[6] M. Araki, K. Akimoto and T. Takenaka, Study of riding assist control enabling self-standing in stationary state, SAE International Journal of Vehicle Dynamics, Stability, and NVH, pp. 47-56, 2018.
[7] M. Kawaguchi and M. Yamakita, Stabilizing of bike robot with variable configured balancer, presented at SICE Annual Conference, 2011.
[8] P. Wang, F. Han, and J. Yi, Gyroscopic balancer-enhanced motion control of an autonomous bikebot, ASME Journal of Dynamic Systems Measurement and Control, vol. 145, issue 10, 2023.
[9] E. Tsujii, M. Tsuchiya, T. Terayama and N. Tsurumi, Study on Self-standing Motorcycle Control Mechanism, in Transactions of the Society of Automotive Engineers of Japan, 50(4), pp. 1049-1054, 2019.
[10] P. Wang, J. Yi, and T. Liu, Stability and control of a rider-bicycle system:Analysis and experiments, IEEE Trans. on Automation Science and Engineering, vol. 17, no. 1, pp. 348-360, 2020.
[11] P. Wang and J. Yi, Balance performance tuning of rider-bikebot interactions, presented at Annual American Control Conference (ACC), June 27-29, 2018.
[12] K. Chen, Y. Zhang, J. Yi, and T. Liu, An integrated physical-learning model of physical human-robot interactions with application to pose estimation in bikebot riding, The International Journal of Robotics Research, vol. 35(12), pp. 1459-1476, April 2016.
[13] T. Takenaka, T. Matsumoto, and T. Yoshiike, Real time motion generation and control for biped robot -1st report: Walking gait pattern generation-, in Proceedings of 2009 IEEE/RSJ International Conference on Intelligent Robots and Systems, 2009, pp. 1084-1091.
[14] T. Takenaka, T. Matsumoto, T. Yoshiike, and S. Shirokura, Real time motion generation and control for biped robot -2nd report: Running gait pattern generation-, IEEE/RSJ International Conference on Intelligent Robots and Systems, pp. 1092-1099, 2009.
[15] T. Takenaka, T. Matsumoto, T. Yoshiike, T. Hasegawa, S. Shirokura, H. Kaneko, and A. Orita, Real time motion generation and control for biped robot -4th report: Integrated balance control-, in Proceedings of IEEE/RSJ International Conference on Intelligent Robots and Systems, 2009, pp. 1092-1099.
[16] T. Takenaka, T. Matsumoto, and T. Yoshiike, Real-time walking gait generation for biped robot, Journal of the Robotics Society of Japan, vol. 29 , no. 5 , pp. 455-462, 2011.
[17] T. Kamioka, H. Kaneko, T. Takenaka, and T. Yoshiike, Simultaneous optimization of ZMP and footsteps based on the analytical solution of divergent component of motion, in Proceedings of 2018 IEEE International Conference on Robotics and Automation, 2018, pp. 1763-1770.
[18] M. A. Hopkins, D. W. Hong, and A. Leonessa, Humanoid locomotion on uneven terrain using the time-varying divergent component of motion, presented at IEEE-RAS 14th International Conference on Humanoid Robots, 2014, pp. 0-6.
[19] G. Romualdi, S. Dafarra, Y. Hu, and D. Pucci, A benchmarking of DCM based architectures for position and velocity controlled walking of humanoid robots, presented at IEEE-RAS 18th International Conference on Humanoid Robots, 2018.
[20] J. Englsberger, C. Ott, and A. Albu-Schaffer, Three-dimensional bipedal walking control using divergent component of motion, in Proceedings of IEEE/RSJ International Conference on Intelligent Robots and Systems, 2013, pp. 2600-2607.
[21] J. Englsberger, G. Mesean, and C. Ott, Smooth trajectory generation and push-recovery based on divergent component of motion, in Proceedings of IEEE/RSJ International Conference on Intelligent Robots and Systems, 2017, pp. 4560-4567.
[22] A. L. Hof, M. G. J. Gazendam, and W. E. Sinke, The condition for dynamics stability, Journal of Biomechanics, vol. 38, pp. 1-8, 2005.
[23] T. Sugihara, Standing stabilizability and stepping maneuver in planar bipedalism based on the best COM-ZMP regulator, in Proceedings of 2009 IEEE International Conference on Robotics and Automation, 2009, pp. 1966-1971.
[24] K. Morishima, and H. Daimoto, Development of evaluation method for the riding skills of motorcycle riders, Human Interface Society, vol. 17 , no. 4 , pp. 385-394, 2015